

# Dynamical Evolution Analysis of Standard Geostationary Transfer Orbits Injected by Chinese Launchers

Yue Wang<sup>1</sup>, Xuhui Luo<sup>2</sup>

<sup>1</sup> School of Astronautics, Beihang University, 37 Xueyuan Road, Haidian District, Beijing, 100083, China

<sup>2</sup> School of Astronautics, Beihang University, 37 Xueyuan Road, Haidian District, Beijing, 100083, China

## Abstract

The dynamical evolution of geostationary transfer orbits (GTOs) is a fundamental issue for the space debris mitigation in this orbit region. The abandoned launch vehicle upper stages in GTOs are a potential source for collisions and future debris in both of the low Earth orbit region and geostationary orbit region. Due to the low perigee and high apogee, GTOs are affected by multiple perturbations and their interactions, including the atmospheric drag, Earth's oblateness, and luni-solar perturbations. As a result, the orbital dynamics are extremely sensitive to initial conditions and other system parameters. The initial inclination and perigee height of GTOs are usually determined by the launch vehicles and launch sites. GTOs belonging to different countries and international organizations have distinct initial orbital elements, and, therefore, have quite different dynamical properties and evolution patterns. In this paper, the dynamical evolution of standard GTOs injected by Chinese Long March 3A series launchers and Long March 5 launcher will be analyzed by numerical studies. Especially, two resonances associated with the solar apparent orbital motion will be identified, and their effects will be investigated. In addition, the dynamical properties of Chinese GTOs will be compared with the low-inclination high-perigee European GTOs. The results will provide useful insights for the space debris mitigation associated with Chinese GTOs.

**Keywords:** Long-term evolution, Orbital lifetime, Geostationary transfer orbits (GTOs), Chinese launchers, Solar resonances

## Introduction

With the increase of satellite launches and space activities, the space around Earth has been becoming more and more crowded with space debris of various sizes, from particles smaller than 1 mm to defunct spacecraft and abandoned rocket bodies of several square meters. According to U.S. Strategic Command, as of end of 2017, more than 23,000 man-made objects in orbit have been catalogued by United States Space Surveillance Network, among which 87% are defunct spacecraft and debris, and 7% are abandoned rocket bodies. The growing number of space debris poses a significant threat to operational spacecraft, e.g., the loss of the operational Iridium-33 satellite caused by collision with the defunct Kosmos-2251 satellite on 10 February 2009. Space debris mitigation has become a global concern for the space community. National and international efforts, such as U.S. Government Orbital Debris Mitigation Standard Practices, Inter-Agency Space Debris Coordination Committee (IADC) Space Debris Mitigation Guidelines, United Nations Space Debris Mitigation Guidelines, French Space Operations Act, and etc., have been made to ensure that the increase of space debris associated with current and future space activities are properly mitigated.

The dynamical evolution of geostationary transfer orbits (GTOs) is an important issue for space debris mitigation. The abandoned launch vehicle upper stages in GTOs, which are large

objects and have large relative velocities with respect to objects in low Earth orbits (LEOs) and geostationary orbits (GEOs), are a potential source for collisions and future debris in both of the LEO region and GEO region, the two most important and populated orbital regions [1]. In this aspect, knowledge of the GTO dynamical evolution under natural perturbations is urgent for predicting the distribution, decay, and lifetime of the space debris in GTOs.

Due to the low perigee and high apogee, GTOs are affected by multiple perturbations and their interactions, including the atmospheric drag, Earth's oblateness, and luni-solar perturbations. Atmospheric drag takes its effect near the perigee, reduces the semi-major axis and eccentricity, but almost does not affect the orbital orientation. With its effect strongly depending on the atmospheric density that is highly uncertain and has large fluctuations, atmospheric drag introduces high uncertainties into the GTO evolution [2], [3]. By rotating the orbital plane and apsidal line, Earth's oblateness has a combined effect with the luni-solar perturbations that depend on the relative positions of the Moon and Sun with respect to the orbital plane and apsidal line. With Earth's oblateness together, the luni-solar perturbations induce an eccentricity (perigee height) oscillation, which is the superposition of a long period of several years and two shorter periods of about 14 days and 180 days (half the orbital periods of the perturbing bodies), respectively [4], [5], [6], [7], [8]. Many works have discussed the effects of luni-solar perturbations, especially the perigee height oscillation, as well as the orbital lifetime reduction [9], [10], [11], [12], [2], [13], [14]. It has been shown that the long-period eccentricity (perigee height) oscillation is induced by the rotation of the GTO's orbital plane and apsidal line, caused mainly by Earth's oblateness, whereas the short-period oscillations are induced by the periodic luni-solar apparent orbital motions [14]. The phases of long- and short-period oscillations are determined by the azimuths of the luni-solar orbital momenta and the luni-solar position vectors with respect to the apsidal line, respectively [14]. With different oscillation phases, the luni-solar perturbations can reduce or enhance the orbital lifetime significantly by lowering or raising the initial perigee.

The 1:1 resonance between the solar apparent orbital motion and the rotation of the orbital apsidal line caused by Earth's oblateness, i.e., the solar apsidal resonance, is another remarkable outcome of the multiple perturbations. With the semi-major axis being reduced by the atmospheric drag, the solar apsidal resonance occurs when the rotation of the orbital apsidal line is commensurate with the solar orbital motion. At the resonance, the solar azimuth with respect to the apsidal line has a U-turn, staying there for a long duration, and the short-period eccentricity oscillation induced by the solar orbital motion becomes monotonically increasing or decreasing. Since different types of resonance have distinct effects on the orbital evolution, and the type of the resonance is difficult to predict, the high dynamic sensitivity with respect to initial conditions and system parameters is introduced into the dynamics [15]. The dynamic sensitivity and the system uncertainties, especially the large intrinsic uncertainty in the atmospheric density, make the deterministic prediction of the GTO's atmospheric reentry fairly impossible. In practice, a statistical approach is required in studies associated with orbital lifetime of GTOs [2], [16].

During the launches of GEO satellites, the initial inclination and perigee height of GTOs are usually determined by the launchers and launch sites: The initial inclination is close to the geographic latitude of the launch site, and the initial perigee height is determined by the mission profile design considering the launcher's capacity. Therefore, GTOs belonging to different countries and international organizations have distinct initial orbital elements. Because of the complicated dynamics and the high dynamic sensitivity, GTOs with different initial inclinations and perigee heights have quite different dynamical properties and evolution patterns, and, therefore, deserve respective investigations.

The Long March 3A (also known as LM-3A, Chang Zheng 3A, and CZ-3A) series launchers, including LM-3A, LM-3B, LM-3BE, and LM-3C, are currently the workhorse launch vehicles for China's GTO launch missions, with a payload capacity of about 2.6-5.5 tonnes to GTO. The Long March 5 (also known as LM-5, Chang Zheng 5, and CZ-5) launcher is a new-generation heavy lift launch vehicle, with a maximum payload capacity of about 14 tonnes to GTO. In its maiden launch on 3 November 2016 from Wenchang Satellite Launch Center, LM-5 successfully delivered the Yuan Zheng 2 (YZ-2) upper stage and the payload into the expected GTO.

In this paper, the dynamical evolution of standard GTOs injected by Chinese launchers, including the GTOs with an inclination of 28.5 degrees launched by LM-3A series from Xichang Satellite Launch Center and the GTOs with an inclination of 19.5 degrees launched by LM-5 from Wenchang Satellite Launch Center, will be analyzed by numerical studies. Especially, two resonances associated with the solar apparent orbital motion will be identified, and their effects will be investigated. In addition, the dynamical properties of Chinese GTOs will be compared with the low-inclination high-perigee GTOs injected by the European Ariane 5 launcher. The results will provide useful insights for the mitigation of space debris in Chinese GTOs.

### Singly-Averaged Orbital Dynamics

In this study, a singularity-free semi-analytical orbital model in terms of Milankovitch elements will be used as the orbital propagator, which accounts for  $J_2$ , luni-solar perturbations with the Hill approximation, and atmospheric drag with the exponential density model [14]. Through an averaging process over the orbital motion in the GTO, associated short-period terms are eliminated and the effect of atmospheric drag assumes a simple analytical form in the variational equations of orbital elements. The averaging process also enables a multi-orbit time step and an improved computational speed. By capturing the main effects of the perturbations, this singly-averaged orbital dynamics (SAOD) can provide a computationally-efficient portrayal for the long-term orbital evolution. A brief description of SAOD will be given in the following.

The Milankovitch elements contains two orthogonal vectors: the orbital angular momentum vector  $\mathbf{H}$  with the magnitude  $\sqrt{\mu a(1-e^2)}$ , normal to the orbital plane, and the Laplace vector  $\mathbf{b} = \mu \mathbf{e}$ , pointing towards perigee, where  $\mu$  is the gravitational constant of Earth,  $a$  is the semi-major axis, and  $\mathbf{e}$  is the eccentricity vector. These two vectors can be written in terms of the position  $\mathbf{r}$  and velocity  $\mathbf{v}$  as

$$\mathbf{H} = \mathbf{r} \times \mathbf{v}, \quad \mathbf{e} = \frac{1}{\mu} \mathbf{v} \times \mathbf{r} \times \mathbf{v} - \frac{\mathbf{r}}{r}, \quad (1)$$

where  $\mathbf{r} \times \mathbf{v} = \mathbf{r} \times \mathbf{v}$  and  $\mathbf{v} \times \mathbf{r} \times \mathbf{v} = \mathbf{v} \times (\mathbf{r} \times \mathbf{v})$ .

The variational equations of  $\mathbf{H}$  and  $\mathbf{e}$  subjected to Earth's oblateness, luni-solar perturbations, and atmospheric drag are given by [14]

$$\begin{aligned}
\dot{\mathbf{H}} &= \dot{\mathbf{H}}_{J_2} + \dot{\mathbf{H}}_S + \dot{\mathbf{H}}_M + \dot{\mathbf{H}}_{Atm} \\
&= -\frac{3\mu J_2 R_E^2}{2a^3 h^5} (\hat{\mathbf{p}} \cdot \mathbf{h}) \hat{\mathbf{p}}^\times \mathbf{h} + \frac{3a^2 \mu_S}{2d_S^3} \left[ 5(\hat{\mathbf{d}}_S \cdot \mathbf{e}) \mathbf{e}^\times \hat{\mathbf{d}}_S - (\hat{\mathbf{d}}_S \cdot \mathbf{h}) \mathbf{h}^\times \hat{\mathbf{d}}_S \right] \\
&\quad + \frac{3a^2 \mu_M}{2d_M^3} \left[ 5(\hat{\mathbf{d}}_M \cdot \mathbf{e}) \mathbf{e}^\times \hat{\mathbf{d}}_M - (\hat{\mathbf{d}}_M \cdot \mathbf{h}) \mathbf{h}^\times \hat{\mathbf{d}}_M \right] \tag{2}
\end{aligned}$$

$$\begin{aligned}
&-\frac{1}{2} \delta \sqrt{\frac{\mu(1-e^2)}{2a\pi z}} \rho_{p_0} \exp\left(\frac{r_{p_0} - r_p}{H_\rho}\right) (1+K_1) \mathbf{H}, \\
\dot{\mathbf{e}} &= \dot{\mathbf{e}}_{J_2} + \dot{\mathbf{e}}_S + \dot{\mathbf{e}}_M + \dot{\mathbf{e}}_{Atm} \\
&= -\frac{3nJ_2 R_E^2}{4a^2 h^5} \left\{ \left[ 1 - \frac{5}{h^2} (\hat{\mathbf{p}} \cdot \mathbf{h})^2 \right] \mathbf{h}^\times + 2(\hat{\mathbf{p}} \cdot \mathbf{h}) \hat{\mathbf{p}}^\times \right\} \mathbf{e} \\
&\quad + \frac{3\mu_S}{2nd_S^3} \left[ 5(\hat{\mathbf{d}}_S \cdot \mathbf{e}) \mathbf{h}^\times \hat{\mathbf{d}}_S - (\hat{\mathbf{d}}_S \cdot \mathbf{h}) \mathbf{e}^\times \hat{\mathbf{d}}_S - 2\mathbf{h}^\times \mathbf{e} \right] \\
&\quad + \frac{3\mu_M}{2nd_M^3} \left[ 5(\hat{\mathbf{d}}_M \cdot \mathbf{e}) \mathbf{h}^\times \hat{\mathbf{d}}_M - (\hat{\mathbf{d}}_M \cdot \mathbf{h}) \mathbf{e}^\times \hat{\mathbf{d}}_M - 2\mathbf{h}^\times \mathbf{e} \right] \\
&\quad - B \frac{1+e}{a\sqrt{2\pi z}} \rho_{p_0} \exp\left(\frac{r_{p_0} - r_p}{H_\rho}\right) (1+K_2) H \hat{\mathbf{e}}, \tag{3}
\end{aligned}$$

where  $R_E$  is the mean equatorial radius of the Earth,  $\mathbf{h} = \mathbf{H} / \sqrt{\mu a}$  is the scaled orbital angular momentum,  $a$  is the semi-major axis,  $n = \sqrt{\mu / a^3}$  is the mean motion of the GTO,  $\hat{\mathbf{p}}$  is the spin axis of Earth,  $\mu_S$  and  $\mu_M$  are gravitational constants of the Sun and Moon, respectively,  $\mathbf{d}_S$  and  $\mathbf{d}_M$  denotes the position vectors of the Sun and Moon relative to Earth, respectively,  $B = SC_D / m$  is the ballistic coefficient of the GTO object,  $S/m$  is the area-to-mass ratio (AMR),  $C_D$  is the non-dimensional drag coefficient with a typical value of 2.2,  $r_p = a(1-e)$ ,  $z = ae / H_\rho$ ,  $H_\rho$  is the constant scale height in the exponential atmospheric density model,  $\rho = \rho_{p_0} \exp[-(r - r_{p_0}) / H_\rho]$ ,  $\rho_{p_0}$  and  $r_{p_0}$  are the atmospheric density and distance from the Earth center at initial perigee, respectively, and

$$K_1 = \frac{1+3e^2}{8z(1-e^2)}, K_2 = \frac{3e^2 - 4e - 3}{8z(1-e^2)}. \tag{4}$$

## Global Pattern of the Orbital Evolution

### Initial Conditions and System Parameters

Two epoches are considered in the simulations: 1 Jan. 2015 00:00:00 UTC and 2 Apr. 2015 06:00:00 UTC, corresponding to two different mean longitudes of the Sun,  $l_S$ , and resulting in two different phase differences between the long-period luni-solar perturbation and the short-period solar perturbation. We will discuss this point in the following.

The initial orbital elements of the GTO injected by LM-3A series, defined at injection, are chosen as the standard mission profile from Xichang Satellite Launch Center,

$$h_{a0} = 35958 \text{ km}, h_{p0} = 200 \text{ km}, i_0 = 28.5 \text{ deg}, \omega_0 = 179.6 \text{ deg}, \quad (5)$$

where  $h_{a0}$  and  $h_{p0}$  are the initial values of the apogee height and perigee height, respectively.\*

The upper stages of LM-3A series are cylinders with length = 12.38 m, diameter = 3 m, and empty mass = 2.8 or 3.06 tons, thus, the AMR  $S/m$  has a range of 0.0023-0.0133 m<sup>2</sup>/kg.† In the simulations, a mean value of 0.0075 m<sup>2</sup>/kg has been chosen.

The initial orbital elements of the GTO injected by LM-5 are given by the second stage's orbit right after the payload separation in its maiden launch from Wenchang Satellite Launch Center,†

$$h_{a0} = 35958 \text{ km}, h_{p0} = 200 \text{ km}, i_0 = 28.5 \text{ deg}, \omega_0 = 179.6 \text{ deg}. \quad (6)$$

The second stage of LM-5 is a cylinder with length = 11.5 m, diameter = 5 m, and empty mass = 3.4 tons, thus, the AMR  $S/m$  has a range of 0.005-0.016 m<sup>2</sup>/kg.† In the simulations, a mean value of 0.01 m<sup>2</sup>/kg has been chosen.

The atmospheric density at the initial perigee  $\rho_{p0}$  and the scale height  $H_p$  in the orbital model SAOD in the cases of  $h_{p0} = 200 \text{ km}$  and  $h_{p0} = 211 \text{ km}$  for LM-3A series and LM-5, respectively, are calculated by using Eqns. (58) and (59) of Ref. 14.

To show global patterns of the orbital evolution, both of the GTOs given by Eqn. (5) and (6) are propagated in the cases of two epoches, with the initial right ascension of the ascending node (RAAN),  $\Omega_0$ , ranging from 0° to 360°, which corresponds to different launch hours during one day. The time step of the simulations is 10,000 seconds. When the perigee height of the GTO is lower than 100 km, the GTO will be regarded to be decayed. Each case is propagated until the GTO is decayed, with a maximum simulation timespan of 100 years.

### Simulation Results and Discussions

The evolution of the perigee height  $h_p$  of GTOs injected by LM-3A series and LM-5 with different  $\Omega_0$  with epoches 1 Jan. 2015 00:00:00 UTC and 2 Apr. 2015 06:00:00 UTC are shown in Figs. 1, 2, 3, and 4, respectively.

Figs. 1-4 show the perigee height oscillations caused by the combined effects of the luni-solar perturbations and Earth's oblateness, and especially, also show a strong dependence of the orbital lifetime on the initial RAAN,  $\Omega_0$ . Changing  $\Omega_0$ , i.e., rotating the orbit about Earth's spin axis in the inertial space, leads to different initial azimuths of the luni-solar orbital momenta and the solar position vector with respect to the orbital apsidal line, and, consequently, leads to different initial phases for the long- and short-period perigee height oscillations [14]. The initial perigee height will be raised or lowered by the luni-solar perturbations. The orbits with different  $\Omega_0$ , which although have the same initial perigee height, will have quite different perigee heights and orbital lifetime during the subsequent evolution.

\* LM-3A Series Launch Vehicles User's Manual, Issue 2011

† <http://www.satlist.nl/>

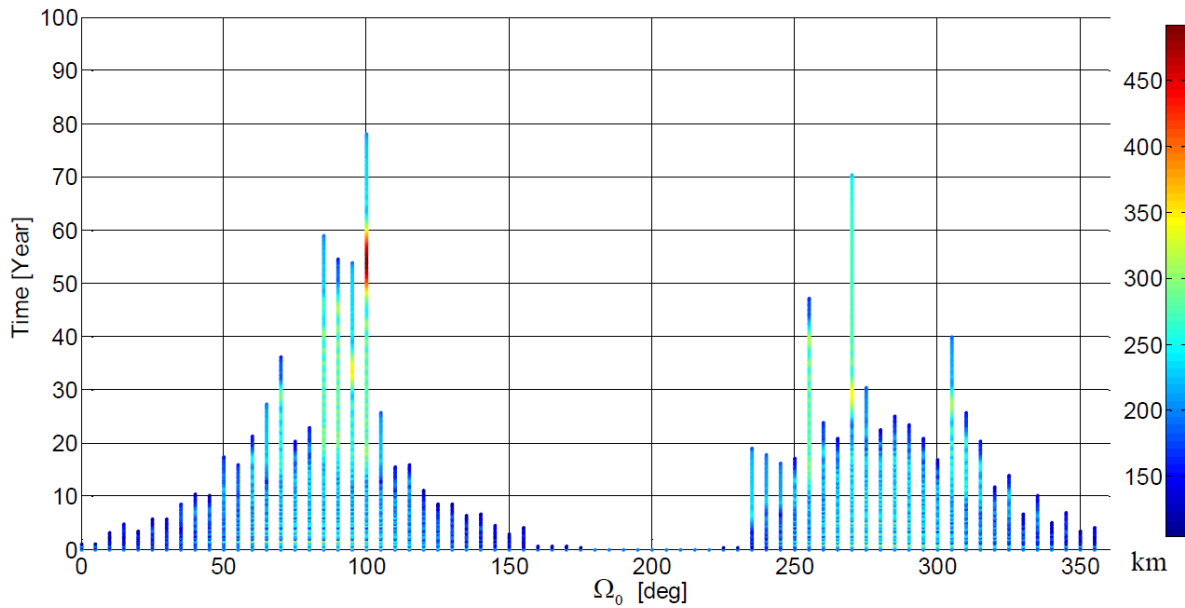


Fig. 1: Evolution of  $h_p$  of LM-3A GTO with different  $\Omega_0$  with epoch 1 Jan. 2015 00:00:00 UTC

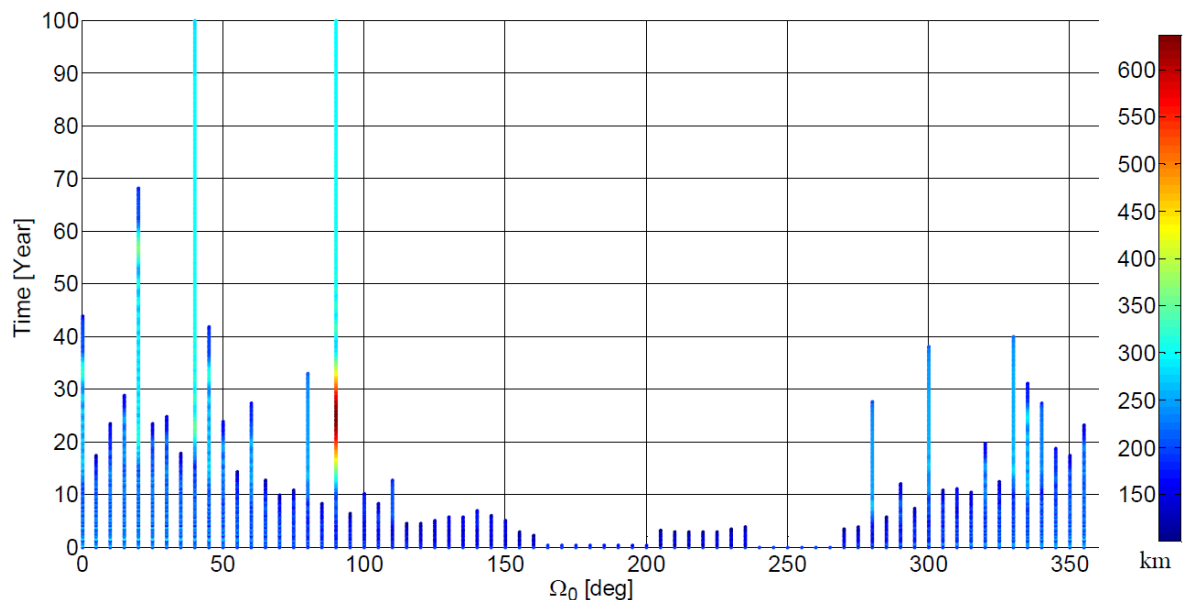


Fig. 2: Evolution of  $h_p$  of LM-3A GTO with different  $\Omega_0$  with epoch 2 Apr. 2015 06:00:00 UTC

More specifically, in the case of epoch 1 Jan. 2015 00:00:00 UTC, the Sun is near the winter solstice. When  $\Omega_0 \approx 0^\circ$  or  $180^\circ$ , the initial azimuth of the solar position vector with respect to the orbital apsidal line is about  $90^\circ$  or  $270^\circ$ , i.e., the initial local time of perigee is about 6 h or 18 h, and then, the short-period perigee height oscillation associated with the solar periodic orbital motion is initially at the beginning of a decrease phase [14]. In the meantime, the long-period perigee height oscillation, which is induced by the luni-solar orbital momenta and the rotation of the GTO, is also nearly at the beginning of a decrease phase [14]. Consequently, the resultant perigee height will oscillate below the initial value, and the orbit decays fast due to the dense atmosphere at the low altitude and has a short lifetime, as shown in Figs. 1 and 3. On the contrary, when  $\Omega_0 \approx 90^\circ$  or  $270^\circ$ , the initial azimuth of the solar position vector with respect to the orbital apsidal line is about  $0^\circ$  or  $180^\circ$ , i.e., the initial local time of perigee is about 12 h or 0 h, and then, the short-period perigee height oscillation is initially at the beginning of an increase phase [14]. The long-period perigee height oscillation is more

complicated: In the case of  $\Omega_0 \approx 90^\circ$ , it is at the middle of an increase phase, whereas, in the case of  $\Omega_0 \approx 270^\circ$ , it is at the middle of a decrease phase [14]. That is, the long-period oscillation nearly does not change the average perigee height when  $\Omega_0 \approx 90^\circ$  or  $270^\circ$ . Due to the raising by the short-period oscillation, the average perigee height is above the initial value, and the orbit has a long lifetime, as shown in Figs. 1 and 3.

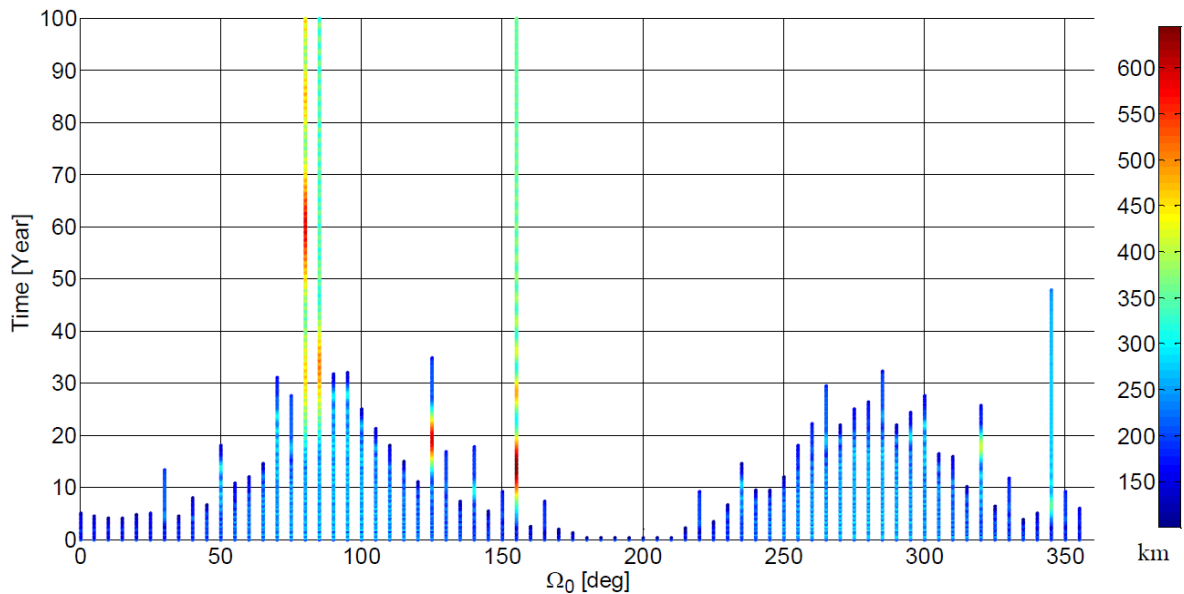


Fig. 3: Evolution of  $h_p$  of LM-5 GTO with different  $\Omega_0$  with epoch 1 Jan. 2015 00:00:00 UTC

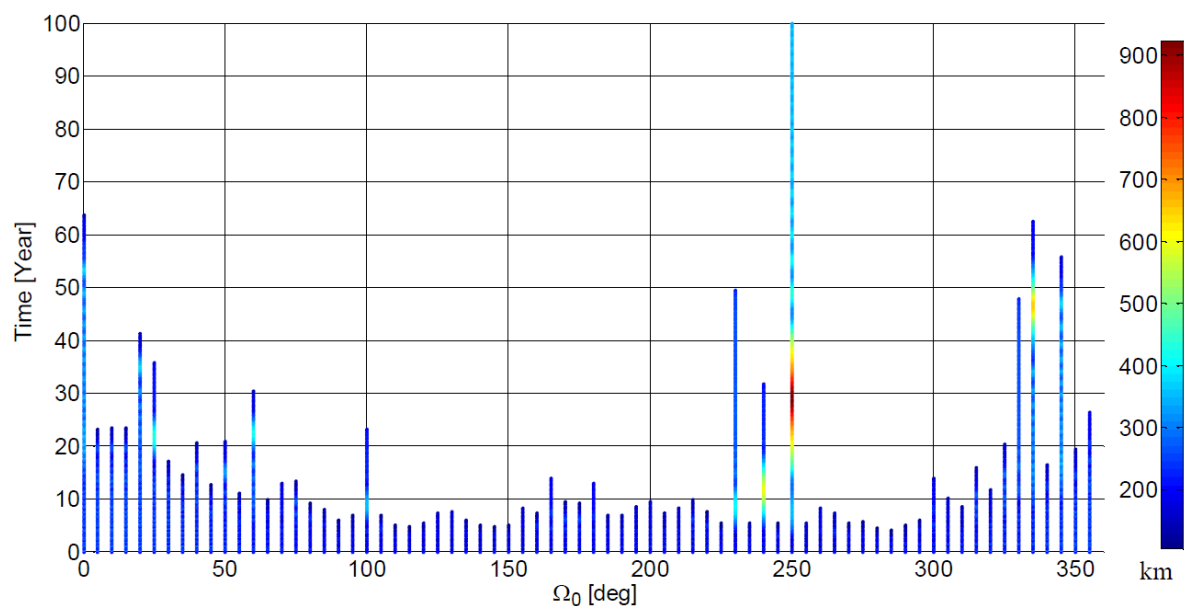


Fig. 4: Evolution of  $h_p$  of LM-5 GTO with different  $\Omega_0$  with epoch 2 Apr. 2015 06:00:00 UTC

Besides  $\Omega_0$ , the initial date is also an important parameter that affects the orbital evolution significantly, as shown by comparisons between Figs. 1 and 2 and between Figs. 3 and 4. The long-period perigee height oscillation will not be affected by a different date, since it is induced by the luni-solar orbital momenta, which are nearly stationary in the inertial space. However, the short-period oscillation will be affected by the initial date directly: With a different initial date, which means a different mean longitude of the Sun,  $l_S$ , the initial solar azimuth with respect to the apsidal line, i.e., the local time of perigee, will be different, resulting in a different initial phase for the short-period oscillation associated with the solar periodic orbital motion [14]. Since the short-period perigee height oscillation has similar

amplitude with the long-period oscillation, the different initial phase of the short-period oscillation alone can result in a quite different oscillation range for the perigee height, and then a quite different orbital evolution.

More specifically, in the case of epoch 2 Apr. 2015 06:00:00 UTC, the Sun is near the spring equinox. Opposite to the case of epoch 1 Jan. 2015 00:00:00 UTC,  $\Omega_0 \approx 0^\circ$  or  $180^\circ$  means that the initial solar azimuth with respect to the orbital apsidal line is about  $0^\circ$  or  $180^\circ$ , i.e., the initial local time of perigee is about 0 h or 12 h, and then, the short-period perigee height oscillation is initially at the beginning of an increase phase;  $\Omega_0 \approx 90^\circ$  or  $270^\circ$  means that the initial solar azimuth with respect to the orbital apsidal line is about  $90^\circ$  or  $270^\circ$  i.e., the initial local time of perigee is about 6 h or 18 h, and then, the short-period perigee height oscillation is initially at the beginning of a decrease phase. Since the long and short-period oscillations has opposite phases when  $\Omega_0 \approx 0^\circ$  or  $180^\circ$ , their effects counterbalance each other to some extent, and the distribution of the perigee height, as well as the orbital lifetime, with respect to  $\Omega_0$  is more uniform than that in the case of epoch 1 Jan. 2015 00:00:00 UTC, as shown by comparisons between Figs. 1 and 2 and between Figs. 3 and 4.

Through comparisons between Figs. 1 and 3 and between Figs. 2 and 4, from a statistic point of view, the orbital lifetime of GTOs injected by LM-3A series is shorter than that of GTOs injected by LM-5. This is because the LM-3A GTO has a lower initial perigee height than LM-5 GTO. By comparing Figs.1 and 3 with Fig. 2 of Ref. 15, it can be also found that, with a higher initial perigee height of 250 km, the GTO injected by European Ariane 5 has a longer orbital lifetime than both of LM-3A series and LM-5 from a statistic point of view. These findings are consistent with the results revealed by statistical studies of Da Costa et al. [12] and Morand et al. [2]: the higher the initial perigee height the higher the orbital life-time.

Several national and international space debris mitigation guidelines have limited the orbital lifetime of objects passing through the LEO region (altitude < 2000 km) to no longer than 25 years after the completion of mission. Results in Figs. 1-4 have shown that, due to the low perigee, the GTOs injected by LM-3A series and LM-5 have a high probability of being compliant with the 25-year lifetime limit. By choosing a launch hour with an initial local time of perigee away from 0 h and 12 h, a lower average perigee height can be achieved by utilizing the solar perturbation, and the probability of being compliant with the 25-year lifetime limit can be much higher.

### **Solar Resonance with $\dot{\Psi}_1 = \dot{\Omega} + \dot{\omega} - \dot{l}_s \approx 0$**

Since  $-\Psi_1 = l_s - \Omega - \omega$  is approximately equal to the solar azimuth with respect to the orbital apsidal line, the solar resonance with  $\dot{\Psi}_1 = \dot{\Omega} + \dot{\omega} - \dot{l}_s \approx 0$  is exactly the solar apsidal resonance, i.e., the 1:1 resonance between the solar apparent orbital motion and the rotation of the orbital apsidal line caused mainly by Earth's oblateness. In the following, we will discuss the solar azimuth instead of  $-\Psi_1 = l_s - \Omega - \omega$ , since the solar azimuth is directly related to the short-period solar perturbation and has a clear physical meaning [14]. The solar apsidal resonance has been classified into three kinds and their distinct effects on the orbital evolution have been studied in details in Ref. 15 for the high-perigee GTOs injected by the European Ariane 5 launcher.

### **Resonance Condition**

The change rates of RAAN and the argument of perigee caused by  $J_2$  are given by [17]

$$\dot{\Omega}_{J_2} = -1.5J_2\sqrt{\mu}R_E^2 \frac{\cos i}{a^{7/2}(1-e^2)^2}, \quad (7)$$

$$\dot{\omega}_{J_2} = 0.75J_2\sqrt{\mu}R_E^2 \frac{5\cos^2 i - 1}{a^{7/2}(1-e^2)^2} \quad (8)$$

With a relatively small semi-major axis, the rotations of the GTO orbital plane and apsidal line are mainly caused by Earth's oblateness, while the effect of the luni-solar perturbations is much weaker: By using Eqns. (12) and (14) in Ref. 18, calculations have shown that the orbit rotation caused by the luni-solar perturbations is only about one fiftieth of that caused by Earth's oblateness. Therefore, we have

$$\dot{\Omega} \approx \dot{\Omega}_{J_2}, \quad \dot{\omega} \approx \dot{\omega}_{J_2}. \quad (9)$$

The resonance condition  $\dot{\Psi}_1 = \dot{\Omega} + \dot{\omega} - \dot{l}_s \approx 0$  can be written as

$$0.75 \frac{J_2\sqrt{\mu}R_E^2}{a^{7/2}(1-e^2)^2} (5\cos^2 i - 2\cos i - 1) \approx \dot{l}_s, \quad (10)$$

where  $\dot{l}_s$  is assumed to be constant.

Since the inclination of the GTO has a small oscillation with amplitude of about  $0.5^\circ$ , the inclination in the resonance condition (10) can be assumed constant [15]. Then, we obtain the resonance condition in terms of  $a$  and  $e$ ,

$$a(1-e^2)^{4/7} = \left[ \frac{3J_2\sqrt{\mu}R_E^2(5\cos^2 i - 2\cos i - 1)}{4\dot{l}_s} \right]^{2/7}. \quad (11)$$

With  $a$  and  $e$  being reduced gradually by the effect of atmospheric drag, the system will cross the resonance condition (11) inevitably. At the cross point, the solar azimuth has an U-turn, the solar apsidal resonance occurs, and the evolution pattern of the GTO has a pronounced change.

### Different Kinds of Resonance

In this study, in addition to the three kinds in Ref. 15, a fourth kind of solar apsidal resonance has been found for low-perigee GTOs injected by LM-3A series and LM-5, during which the entire U-turn of solar azimuth is within the interval where the solar gravity decreases the eccentricity, and the perigee is raised persistently by the solar gravity.

This fourth kind of solar apsidal resonance cannot exist for high-perigee GTOs, such as the ones injected by the European Ariane 5 launcher [15]. This is because, if the perigee is raised at the beginning of the resonance, the atmospheric drag is reduced significantly, and the rotation of the orbit and the solar azimuth keep nearly constant speeds. Sooner or later, the solar azimuth will enter the nearby interval, and the resonance will belong to the second kind.

However, for low-perigee GTOs, such as the ones studied here, although the perigee is raised at the beginning, the atmospheric drag is still strong enough to shrink the orbit and speed up the orbit rotation. As a result, the entire U-turn of the solar azimuth can finish within the interval where the solar gravity decreases the eccentricity, and, that is, the fourth kind of resonance can exist. From the point of view of space debris mitigation, because of the

persistent perigee raising, the fourth kind of resonance weakens the advantages of low-perigee GTOs.

Table 1 is a summary of the solar apsidal resonance, among which the fourth kind is newly found in this study. In the following, the evolution of two sample GTOs with specific epoch and  $\Omega_0$ , injected by LM-3A series and LM-5, respectively, will be given for each kind of solar apsidal resonance.

Table 1: Four kinds of solar apsidal resonance

Kind of Resonance	Location of U-turn of Solar Azimuth	Perigee Height Variation
First Kind	The entire U-turn occurs in interval where the solar gravity increases eccentricity.	The perigee is lowered by the solar gravity persistently.
Second Kind	U-turn begins in interval where the solar gravity decreases eccentricity, but ends in a nearby interval.	The perigee is first raised by the solar gravity, but then lowered.
Third Kind	Most part of U-turn occurs in the interval where the solar gravity increases eccentricity, but the middle part occurs in a nearby interval.	The perigee is first lowered by the solar gravity, then slightly raised, and finally lowered again.
Fourth kind	The entire U-turn occurs in interval where the solar gravity decreases eccentricity.	The perigee is raised by the solar gravity persistently.

### First Kind of Resonance

Time histories of the solar azimuth and  $h_p$  for the two examples of the first kind of resonance are given in Figs. 5 and 6, respectively.

### Second Kind of Resonance

Time histories of the solar azimuth and  $h_p$  for the two examples of the second kind of resonance are given in Figs. 7 and 8, respectively.

### Third Kind of Resonance

Time histories of the solar azimuth and  $h_p$  for the two examples of the third kind of resonance are given in Figs. 9 and 10, respectively.

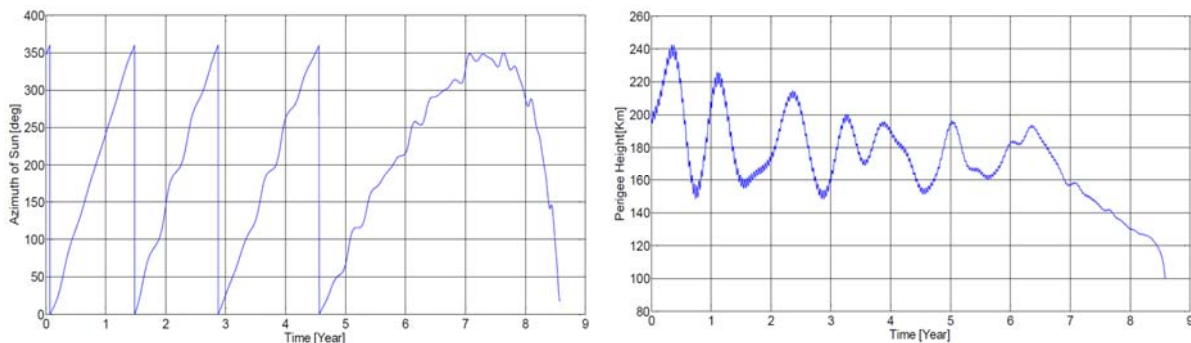


Fig. 5: Time histories of the solar azimuth and  $h_p$  of LM-3A series GTO with epoch 1 Jan. 2015 00:00:00 UTC and  $\Omega_0 = 130^\circ$

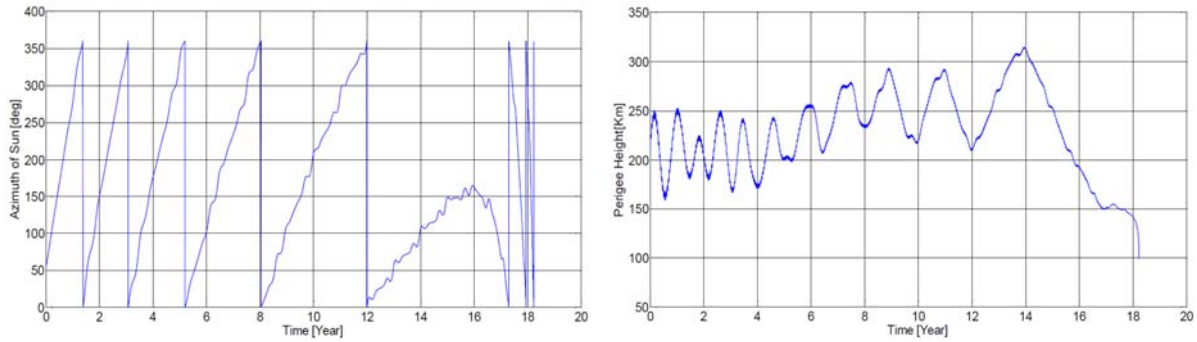


Fig. 6: Time histories of the solar azimuth and  $h_p$  of LM-5 GTO with epoch 1 Jan. 2015 00:00:00 UTC and  $\Omega_0 = 50^\circ$

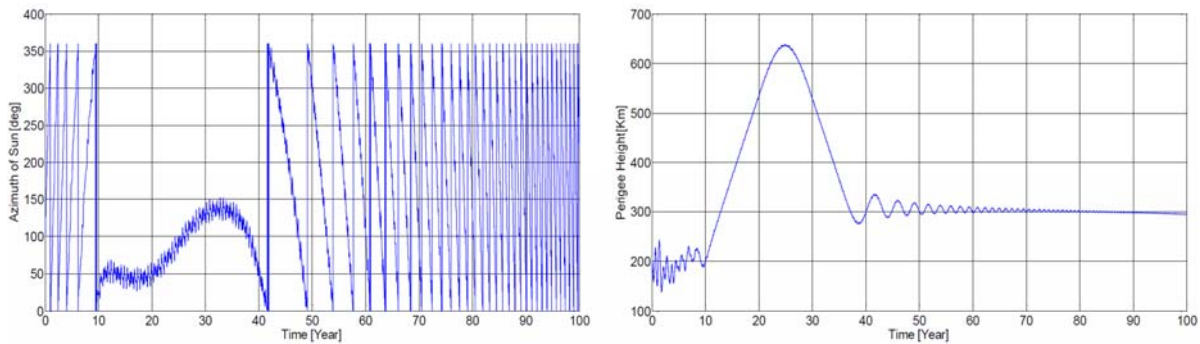


Fig. 7: Time histories of the solar azimuth and  $h_p$  of LM-3A series GTO with epoch 2 Apr. 2015 06:00:00 UTC and  $\Omega_0 = 90^\circ$

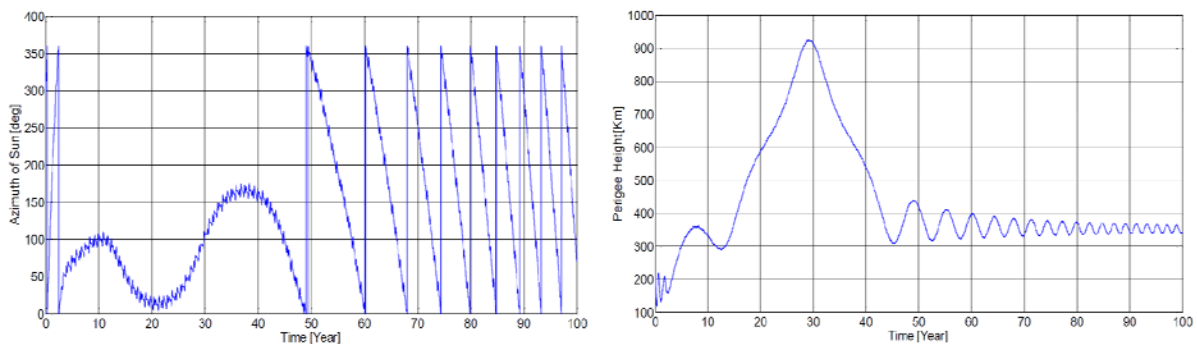


Fig. 8: Time histories of the solar azimuth and  $h_p$  of LM-5 GTO with epoch 1 Apr. 2015 06:00:00 UTC and  $\Omega_0 = 250^\circ$

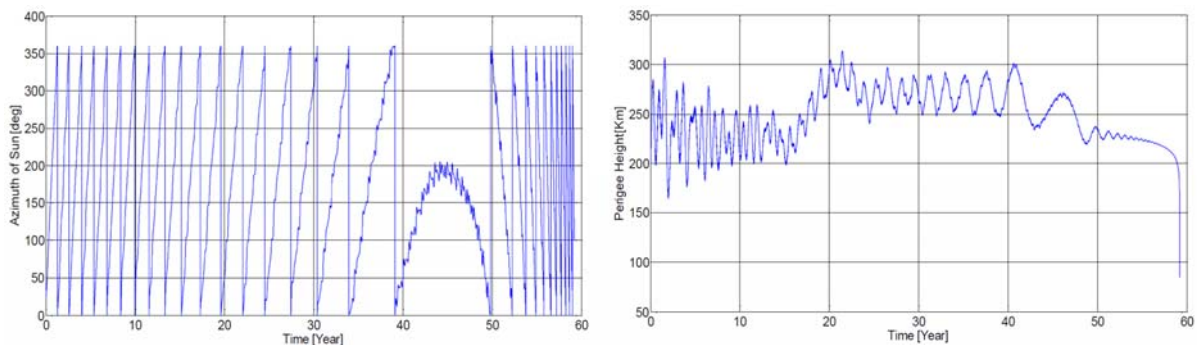


Fig. 9: Time histories of the solar azimuth and  $h_p$  of LM-3A series GTO with epoch 1 Jan. 2015 00:00:00 UTC and  $\Omega_0 = 85^\circ$

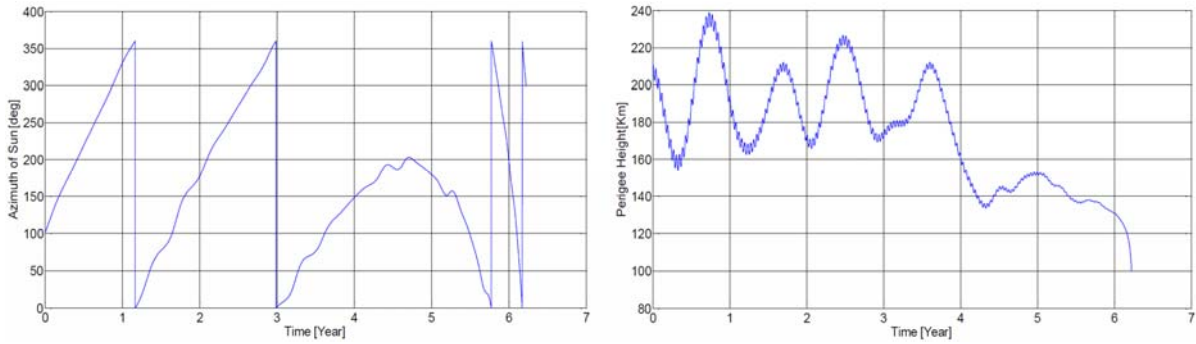


Fig. 10: Time histories of the solar azimuth and  $h_p$  of LM-5 GTO with epoch 2 Apr. 2015 06:00:00 UTC and  $\Omega_0 = 90^\circ$

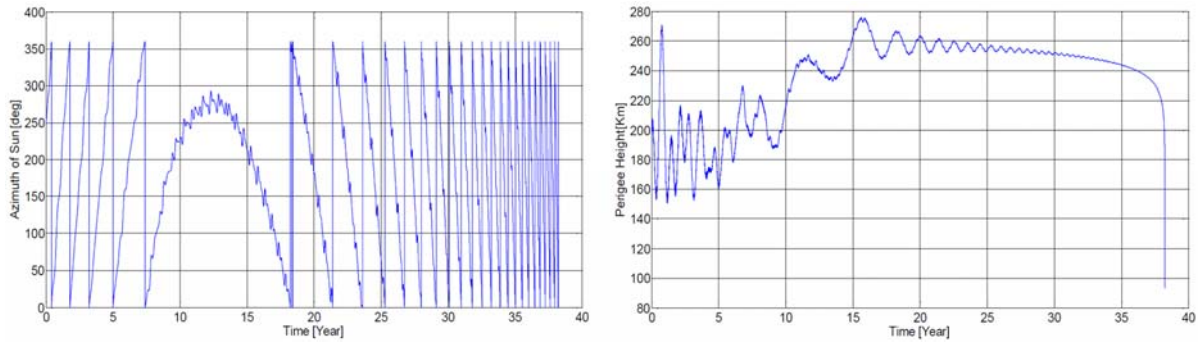


Fig. 11: Time histories of the solar azimuth and  $h_p$  of LM-3A series GTO with epoch 2 Apr. 2015 06:00:00 UTC and  $\Omega_0 = 300^\circ$

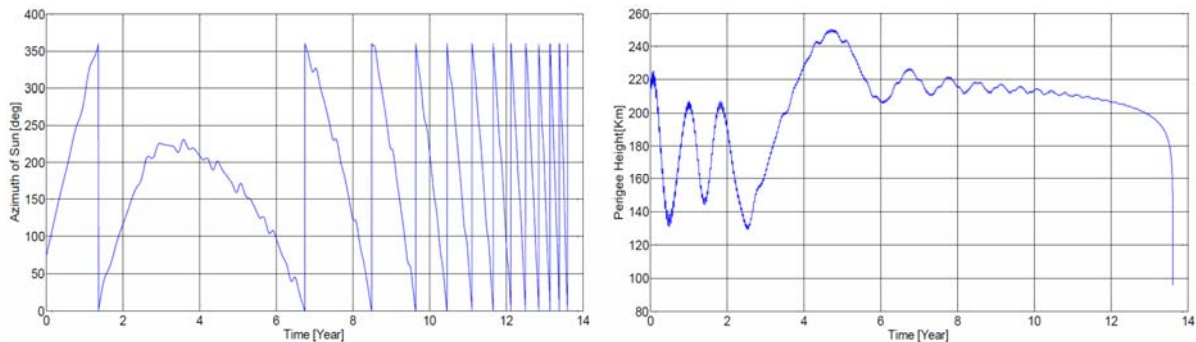


Fig. 12: Time histories of the solar azimuth and  $h_p$  of LM-5 GTO with epoch 1 Jan. 2015 00:00:00 UTC and  $\Omega_0 = 30^\circ$

#### Fourth Kind of Resonance

Time histories of the solar azimuth and  $h_p$  of the fourth kind of resonance are given in Figs. 11 and 12, respectively. It can be seen that the entire U-turn of the solar azimuth is within the interval  $[180^\circ, 270^\circ]$ , where the solar gravity decreases the eccentricity, and the perigee is raised persistently. As a result, the orbital lifetime is extended significantly.

#### Solar Resonance with $\dot{\Omega} + 2\dot{\omega} - 2\dot{l}_s \approx 0$

Besides the solar apsidal resonance with  $\dot{\Psi}_1 = \dot{\Omega} + \dot{\omega} - \dot{l}_s \approx 0$ , the solar resonance with  $\dot{\Psi}_2 = \dot{\Omega} + 2\dot{\omega} - 2\dot{l}_s \approx 0$  is another solar resonance that has noteworthy effects on low-inclination GTOs [2].

#### Resonance Condition

18<sup>th</sup> Australian Aerospace Congress, 24-28 February 2019, Melbourne

By using the same method as in last section, the condition of the solar resonance with  $\Psi_2$

$$\dot{\Psi}_2 = \dot{\Omega} + 2\dot{\omega} - 2\dot{l}_s \approx 0, \quad (12)$$

can be written in terms of  $a$  and  $e$  as follows:

$$a(1-e^2)^{4/7} = \left[ \frac{3J_2\sqrt{\mu}R_E^2(5\cos^2 i - \cos i - 1)}{4\dot{l}_s} \right]^{2/7} \quad (13)$$

### Simulation Results and Discussions

The evolution of four sample GTOs with specific epoch and  $\Omega_0$ , two injected by LM-3A series and two injected by LM-5, will be given to illustrate the solar resonance with  $\dot{\Psi}_2 \approx 0$  and its effects on the orbital evolution.

Time histories of  $\Psi_2$ ,  $h_p$ ,  $i$ , and the trajectory of GTO in the  $a-e$  plane of LM-3A series GTOs, with epoch 1 Jan. 2015 00:00:00 UTC and  $\Omega_0 = 100^\circ$  and with epoch 2 Apr. 2015 06:00:00 UTC and  $\Omega_0 = 20^\circ$ , and LM-5 GTOs, with epoch 1 Jan. 2015 00:00:00 UTC and  $\Omega_0 = 80^\circ$  and with epoch 2 Apr. 2015 06:00:00 UTC and  $\Omega_0 = 21^\circ$ , are given by Figs. 13, 14, 15, and 16, respectively.

Figs. 13-16 show that the resonance occurs at the U-turn of the angle  $\Psi_2$ , where  $\Psi_2$  stays there for a long duration. The periodic term in the variational equations of orbital elements associated with  $\Psi_2$ , i.e., the cosine or sine term having argument of  $\Psi_2$ , changes into a quasi-secular term, and the orbital elements have monotonic changes. This is the underlying dynamical mechanism of the solar resonance with  $\dot{\Psi}_2 \approx 0$ .

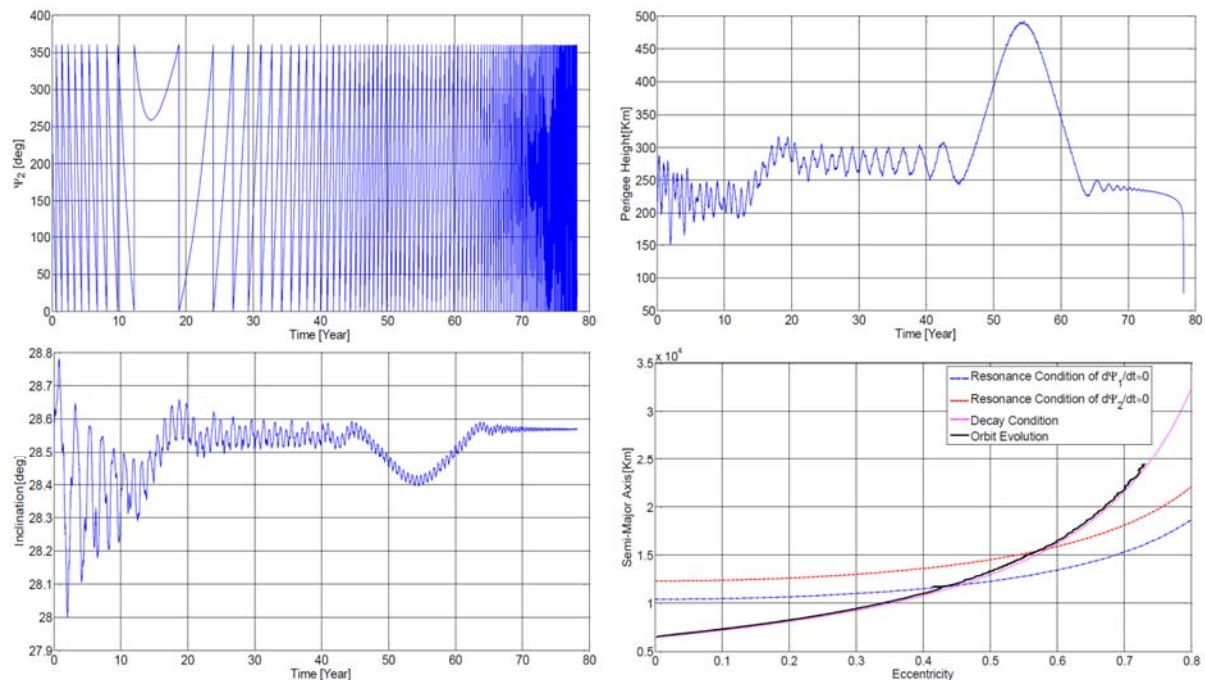


Fig. 13: Time histories of  $\Psi_2$ ,  $h_p$ ,  $i$ , and trajectory in  $a-e$  plane of LM-3A series GTO with epoch 1 Jan. 2015 00:00:00 UTC and  $\Omega_0 = 100^\circ$

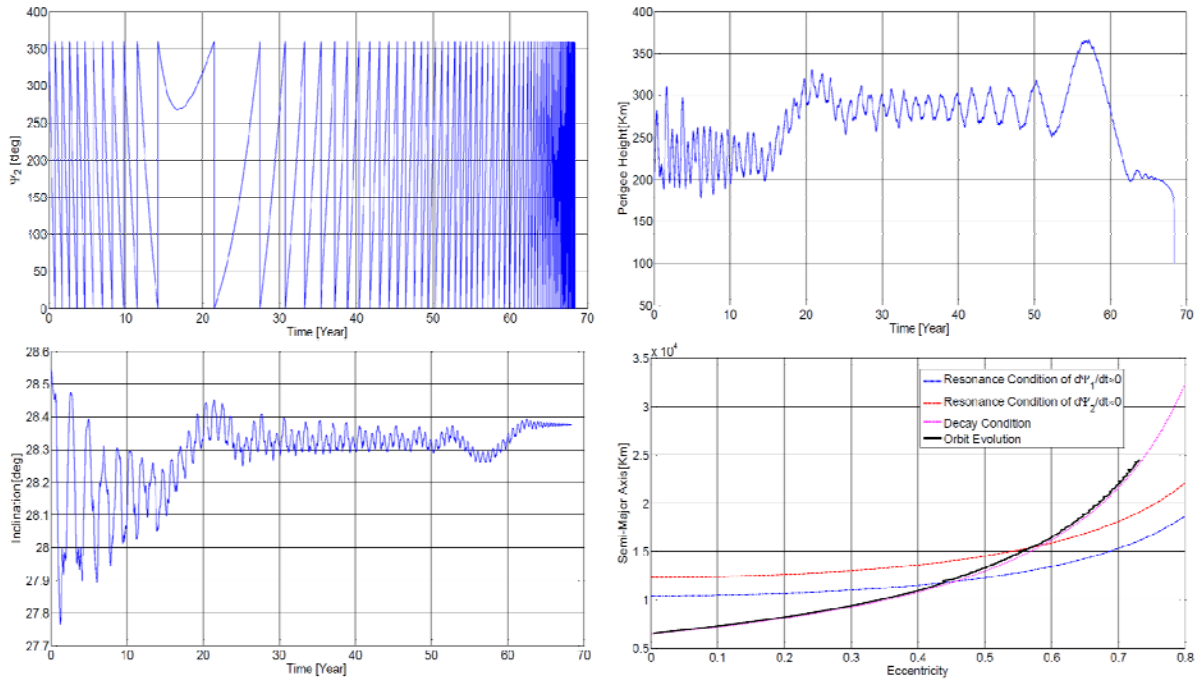


Fig. 14: Time histories of  $\Psi_2$ ,  $h_p$ ,  $i$ , and trajectory in  $a$ - $e$  plane of LM-3A series GTO with epoch 2 Apr. 2015 06:00:00 UTC and  $\Omega_0 = 20^\circ$

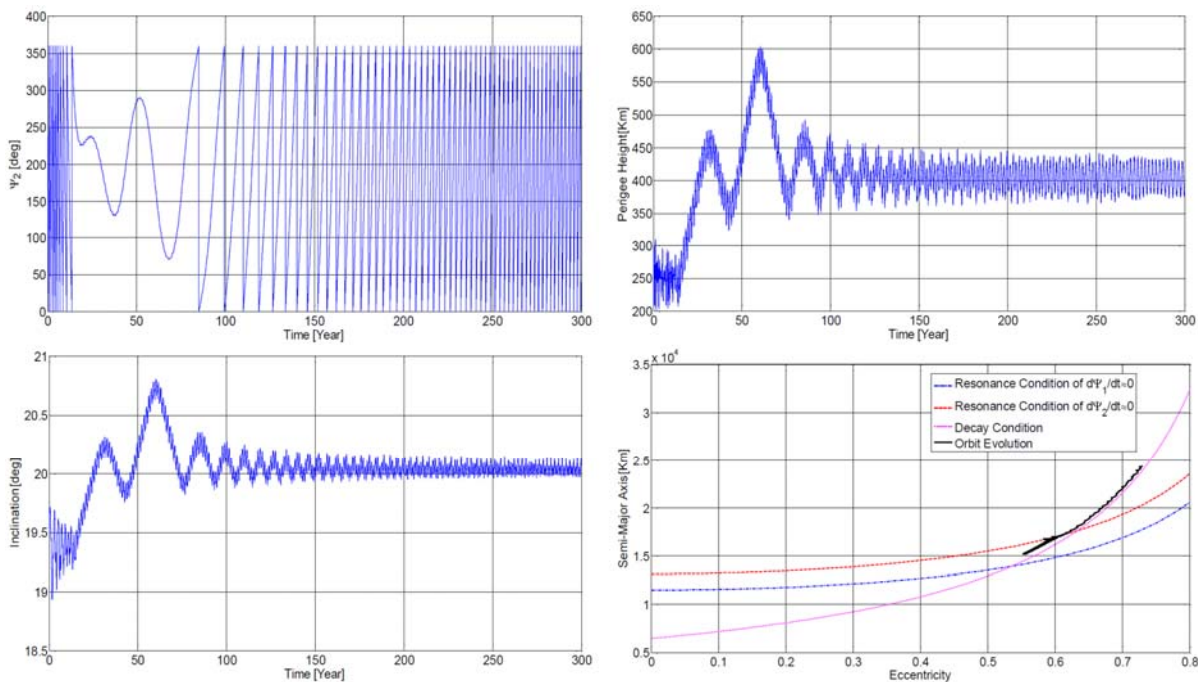


Fig. 15: Time histories of  $\Psi_2$ ,  $h_p$ ,  $i$ , and trajectory in  $a$ - $e$  plane of LM-5 GTO with epoch 1 Jan. 2015 00:00:00 UTC and  $\Omega_0 = 80^\circ$

Another observation is that the solar resonance with  $\dot{\Psi}_2 \approx 0$  is also inevitable for the GTO evolution, like the solar apsidal resonance with  $\dot{\Psi}_1 \approx 0$ , and occurs always before the solar apsidal resonance, as shown by the trajectories in  $a$ - $e$  plane in Figs. 13-16.

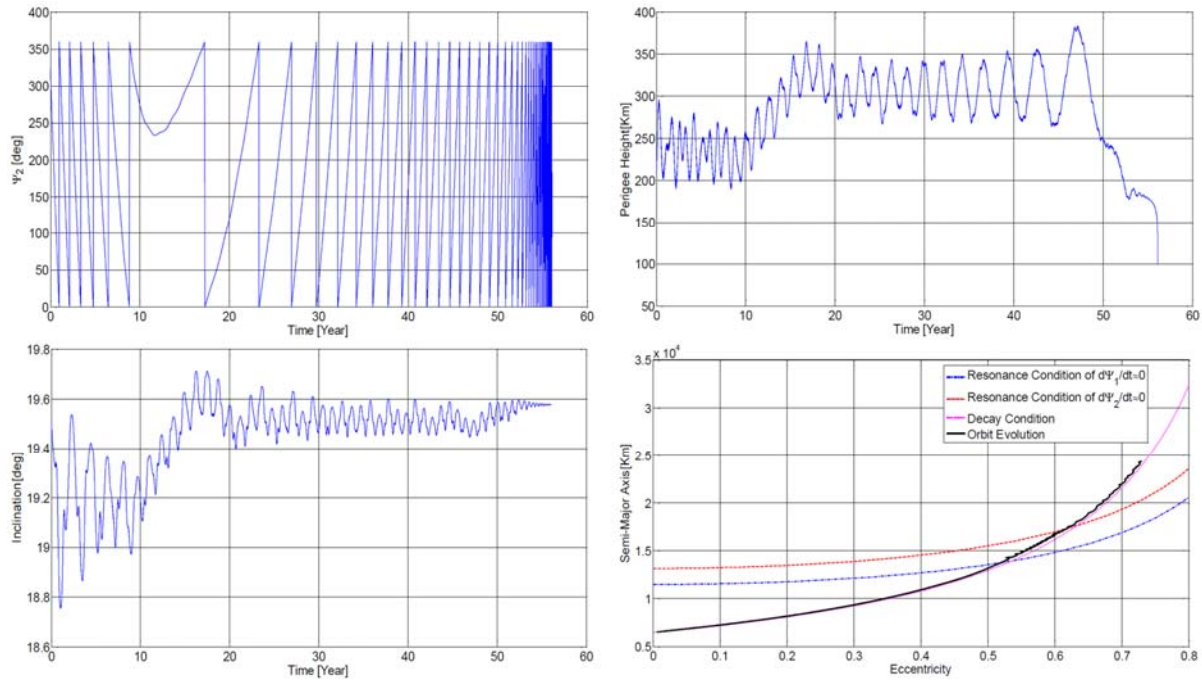


Fig. 16: Time histories of  $\Psi_2$ ,  $h_p$ ,  $i$ , and trajectory in  $a$ - $e$  plane of LM-5 GTO with epoch 2 Apr. 2015 06:00:00 UTC and  $\Omega_0 = 345^\circ$

As shown by time histories of  $h_p$  and  $i$  in Figs. 13-16, the effects of the solar resonance with  $\dot{\Psi}_2 \approx 0$  on the orbital evolution depend on the interval where the U-turn of the angle  $\Psi_2$  occurs: When the U-turn of  $\Psi_2$  occurs in the interval  $[180^\circ, 360^\circ]$ , both the perigee height  $h_p$  and inclination  $i$  are increased by the solar gravity; when the U-turn of the angle  $\Psi_2$  occurs in the interval  $[0^\circ, 180^\circ]$ , both the perigee height  $h_p$  and inclination  $i$  are decreased by the solar gravity. Figs. 13, 14, and 16 show that the orbital lifetime can be extended significantly by the perigee raising caused by the resonance. Fig. 15 shows that the angle  $\Psi_2$  may have multiple U-turns during the resonance, and the perigee height  $h_p$  and inclination  $i$  can be increased or decreased, depending on the interval where the angle  $\Psi_2$  stays.

## Conclusion

Dynamical evolution of the GTOs injected by Chinese Long March 3A series launchers and Long March 5 launcher have been analyzed by numerical studies using a singly-averaged orbital dynamical model. Several important conclusions can be drawn based on the numerical results.

Global orbital evolutions with different  $\Omega_0$  and epoches have shown that the orbital lifetime strongly depends on  $\Omega_0$ , which determines the orientation of the orbital apsidal line in the inertial space and then determines the initial phase of perigee height oscillation caused by the luni-solar perturbations. Consequently, the orbits with different  $\Omega_0$ , although having the same initial perigee height, will have quite different perigee heights and orbital lifetime during the subsequent evolution. Another important parameter that affects the orbital evolution significantly is the initial date, which determines the solar position and then, with a given  $\Omega_0$ , determines the initial phase of the short-period perigee height oscillation associated with the solar orbital motion. If the Sun is initially near the summer or winter solstices, the long- and short-period perigee height oscillations have nearly the same initial phase, and their effects

enhance each other. The distribution of the perigee height, as well as the orbital lifetime, with respect to  $\Omega_0$  is quite nonuniform, centralized at some points. On the contrary, if the Sun is initially near the spring or autumn equinoxes, the long- and short-period perigee height oscillations counterbalance each other, and the distribution of the perigee height, as well as the orbital lifetime, with respect to  $\Omega_0$  is much more uniform.

Due to the lower initial perigee height, the GTOs injected by LM-3A series and LM-5 have a shorter orbital lifetime than the GTO injected by European Ariane 5 from a statistic point of view. Numerical results also show that the GTOs injected by LM-3A series and LM-5 have a high probability of being compliant with the 25-year lifetime limit. If choose a favorable launch hour with an initial local time of perigee away from 0 h and 12 h, a lower perigee height can be achieved, and the probability of being compliant with the 25-year lifetime limit can be even higher.

In the study of the solar apsidal resonance with  $\dot{\Psi}_1 \approx 0$ , the fourth kind of the resonance is found for the GTOs injected by LM-3A series and LM-5, in which the entire U-turn of solar azimuth is within the interval where the solar gravity decreases the eccentricity, and the perigee is raised persistently by the solar gravity. This kind of solar apsidal resonance cannot exist for higher-perigee GTOs, such as the ones injected by the European Ariane 5. From the point of view of space debris mitigation, because of the persistent perigee raising, this fourth kind of resonance weakens the advantages of low-perigee GTOs.

Besides the solar resonance with  $\dot{\Psi}_1 \approx 0$  the solar resonance with  $\dot{\Psi}_2 \approx 0$  is another one that has noteworthy effects on dynamical evolution of GTOs. Numerical results have revealed the solar resonance with  $\dot{\Psi}_2 \approx 0$  and its significant effects for GTOs injected by LM-3A series and LM-5. The resonance increases both of the perigee and inclination if the U-turn of  $\Psi_2$  occurs in the interval  $[180^\circ, 360^\circ]$ , and decreases both of the perigee and inclination if the U-turn occurs in the interval  $[0^\circ, 180^\circ]$ .

## Acknowledgments

The authors acknowledge the support of Fundamental Research Funds for the Central Universities.

## References

1. Klinkrad, H., *ESA Space Debris Mitigation Handbook*, European Space Agency, Darmstadt, Germany, 2003.
2. Morand, V., Le Fèvre, C., Lamy, A., Fraysse, H., and Deleflie, F., “Dynamical Properties of Geostationary Transfer Orbits over Long Time Scales: Consequences for Mission Analysis and Lifetime Estimation,” *AIAA/AAS Astrodynamics Specialist Conference*, No. AIAA 2012-4968, Minneapolis, Minnesota, 13-16 August, 2012.
3. David, E. and Braun, V., “Re-entry Analysis Comparison with Different Solar Activity Models of Spent Upper Stage Using ESA’s DRAMA Tool,” *The 6th IAASS Conference*, Montreal, Canada, 21-23 May, 2013.

4. Shute, B. E., "Prelaunch Analysis of High Eccentricity Orbits," Tech. Rep. NASA Technical Note, NASA TN D-2530, NASA Goddard Space Flight Center, 1964.
5. Paddack, S. and Shute, B., "IMP-C Orbit and Launch Time Analysis," Tech. Rep. Doc. No. X-643-65-40, NASA Goddard Space Flight Center, 1965.
6. Shute, B. E. and Chiville, J., "Lifetimes of Highly Eccentric Satellites," Tech. Rep. Doc. No. X-643-65-402, NASA Goddard Space Flight Center, 1965
7. Shute, B. E. and Chiville, J., "The Lunar-Solar Effect on the Orbital Lifetimes of Artificial Satellites with Highly Eccentric Orbits," *Planetary and Space Science*, Vol. 14, No. 4, 1966, pp. 361-369.
8. Cook, G. E. and Scott, D. W., "Lifetimes of Satellites in Large-Eccentricity Orbits," *Planetary and Space Science*, Vol. 15, No. 10, 1967, pp. 1549-1556.
9. Siebold, K. and Reynolds, R., "Lifetime Reduction of a Geosynchronous Transfer Orbit with the Help of Lunar-Solar Perturbations," *Advances in Space Research*, Vol. 16, No. 11, 1995, pp. 155-161.
10. Takano, A., Tajima, T., and Kanoh, Y., "Recent Efforts Toward the Minimization of GTO Objects and Its Practices in NASDA," *Acta Astronautica*, Vol. 40, No. 11, 1997, pp. 807-813.
11. Sharma, R., Bandyopadhyay, P., and Adimurthy, V., "Consideration of Lifetime Limitation for Spent Stages in GTO," *Advances in Space Research*, Vol. 34, No. 5, 2004, pp. 1227-1232.
12. Da Costa, B. C., Bernardini, M., Cerf, M., Fessard, M., and Reynaud, S., "Long-Term Semi-Analytical Orbit Propagation Tool for Future European Launchers Design," *AIAA/AAS Astrodynamics Specialist Conference*, No. AIAA 2012-4743, Minneapolis, Minnesota, 13-16 August, 2012.
13. Lamy, A., Le Fèvre, C., and Sarli, B., "Analysis of Geostationary Transfer Orbit Long Term Evolution and Lifetime," *Journal of Aerospace Engineering, Sciences and Applications*, Vol. 4, No. 3, 2012, pp. 12-27.
14. Wang, Y. and Gurfil, P., "Dynamical Modeling and Lifetime Analysis of Geostationary Transfer Orbits," *Acta Astronautica*, Vol. 128, 2016, pp. 262-276.
15. Wang, Y. and Gurfil, P., "The Role of Solar Apsidal Resonance in the Evolution of Geostationary Transfer Orbits," *Advances in Space Research*, Vol. 59, No. 8, 2017, pp. 2101-2116.
16. Le Fèvre, C., Fraysse, H., Morand, V., Lamy, A., Cazaux, C., Mercier, P., Dental, C., Deleflie, F., and Handschuh, D., "Compliance of Disposal Orbits with the French Space Operations Act: The Good Practices and the STELA Tool," *Acta Astronautica*, Vol. 94, No. 1, 2014, pp. 234-245.
17. Battin, R. H., *An Introduction to the Mathematics and Methods of Astrodynamics*, American Institute of Aeronautics and Astronautics, Reston, VA, 1987.

18. Stefanelli, L. and Metris, G., “Solar gravitational perturbations on the dynamics of MEO: Increase of the eccentricity due to resonances,” *Advances in Space Research*, Vol. 55, No. 7, 2015, pp. 1855-1867.